Ninth International Symposium on Marine Propulsors
smp'26, St. John's, NL, Canada, July 2026

A practical method to assess the risk for cavitation erosion during automated propeller design optimization

Joost Moulijn[1], Evert-Jan Foeth[1] and John Huisman[1]

[1]Maritime Research Institute Netherlands (MARIN), Wageningen, The Netherlands

ABSTRACT

This paper presents a method that can assess the risk on cavitation erosion during automated propeller design optimization. It is important to include a constraint that the cavitation is not erosive, as a good optimizer will exploit any design freedom to maximize the design targets.

The practical method that is described in this paper uses the planform of the cavity, and its development over time while the blade rotates through the ship's wake, to assess if the cavitation is acceptable. It is based on practical considerations that mimic the judgement of a propeller designer, together with more physical arguments that are underlying to this judgement.

The erosion criterion is deployed in a design optimization task that maximizes efficiency and minimizes the underwater radiated noise (URN) of a propeller. This leads to a Pareto front that represents the trade-off between efficiency and URN. The same optimization is done with passive and active erosion criterion. The criterion effectively avoids propeller designs with erosive cavitation, but that goes to the cost of less efficient and/or more noisy propellers. It limits the tip unloading of the propellers.

Keywords

Cavitation erosion, Propeller design optimization, Under water radiated noise.

1 INTRODUCTION

During the past decades, automated propeller optimization has become increasingly popular. Several authors (Vesting, 2015), (Huisman & Foeth, 2017) have presented optimization frameworks that can optimize for multiple design goals, such as propeller efficiency, hull pressure fluctuations and under water radiated noise (URN), subject to several constraints like mass, class requirements for blade strength, and CPP blades that must be able to pass each other when reversing the pitch. Furthermore, the optimization process may consider several relevant operating conditions (Huisman et al. (2024)).

This paper deals with the important design constraint that the cavitation on the propeller should not lead to erosion of the propeller blade surface. Several authors have shown methods to assess cavitation erosion that are based on advanced CFD simulations (Schenke et al., 2019), (Melissaris et al., 2019). Though very promising, it will take many years before they become feasible for optimizations where thousands or even more design alternatives are considered. Therefore, this paper follows a strongly simplified yet practical approach to cavitation erosion assessment. Eventually, CFD simulation will replace the present method.

Several authors have presented simple methods that use the results of computationally efficient BEM codes to assess the erosion risk. Vesting (2015) introduced a cavity centroid criterion whereby the center of the cavity volume is given a harm factor based on its location on the blade, in addition to a criterion based on the cavity thickness. Gypa et al. (2023) used interactive genetic algorithms, whereby the cavitation topology at the instance of its maximum volume was assessed by an experienced designer to train a surrogate model simulating the designer.

The method in this paper loosely follows principles that are described in "The EROCAV observation handbook" by Bark et al. (2004), as well as propeller design criteria that were developed in the EROSION working groups of the Cooperative Research Ships (CRS) consortium. It uses the outline of the sheet cavitation that is predicted by MARIN's panel code PROCAL (Vaz & Bosschers, 2006) to assess if the cavitation is acceptable or not.

The method is probably too simple to accurately distinguish between erosive and non-erosive cavitation, but it can steer the automated optimization process away from (obviously) erosive cavitation. When a constraint like this is not included, it is highly likely that the optimization process will converge towards designs that suffer from erosive cavitation, as the optimizer will exploit any design freedom to find optima.

[*] Leave blank the last 2.0 cm on the first page for the editors to place some additional information about this paper in a footnote on the first page if necessary.

2 CAVITATION EROSION CRITERA

The judgement of whether cavitation is erosive or not is a complex matter. It is often a rather subjective opinion of the observing cavitation experts. During the last decades significant progress has been made thanks to new high-speed video observation techniques. "The EROCAV observation handbook" by Bark et al. (2004) provides an important step towards further objectivation of judging the erosiveness of cavitation. On the other hand, this scientific work is often too extensive for application in the daily design and consultancy practice.

Bark et al. (2004) describe many cavitation types with various degrees of erosivity. Most erosive are large sheet cavities that separate from the leading edge of the blade (upstream desinence), followed by an accelerated collapse on the mid-chord to trailing edge region of the blade. The behavior of such cavities is difficult to predict with the BEM code PROCAL that is used in MARIN's propeller design and optimization framework, but they can be efficiently avoided by applying a sufficient margin between the fully wetted pressure and the vapor pressure in the mid chord region. The same applies to other undesirable cavitation forms such as bubble and blade-root cavitation.

2.1 Suction Side Cavitation

The cavitation criterion in this paper applies to suction side sheet cavitation that remains attached to the leading edge of the blade. A well-behaving sheet cavity is usually observed to start in the mid-span around 0.7R radius when the blade rotates into the wake peak from the ship's boundary layer. At first, the cavity sheet does not necessarily extend towards the blade tip. When the blade continues to rotate into the ship's wake, it grows in chord-wise direction and also in radial direction towards the tip. The cavity shifts towards the tip of the blade where it merges with the tip vortex. The tip vortex has an important stabilizing effect on the cavity, as discussed below. When the blade leaves the ship's wake the cavity sheet should withdraw towards the blade tip and leading edge. Finally, the cavity leaves the blade as a cavitating tip vortex.

It is complex to capture such behavior in a criterion that can be evaluated by a computer without human interpretation based on the cavity topology alone. Maybe, this can be done by means of artificial intelligence (Gypa et al., 2023). For the present method we go back to a more physical understanding of why the above described behavior is not erosive. First the criterion is described. Thereafter, the underlying ideas to the criterion are presented.

The suction side erosion criterion is a two-step criterion. First the angular speed of cavity closure line (i.e. the trailing edge of the sheet cavity, see Figure 1) is checked for each time step and radius. When the ratio of the closure line speed and the propeller rotational speed is sufficiently small the cavity is not erosive (at that time-step and radius). This typically occurs when the blade is rotating into the wake peak, and the sheet cavity is growing in chord-wise direction. This first step is mathematically expressed as:

$$\frac{\omega_{cav\,r,t}}{\omega_{prop}} < SR_{max} \tag{1}$$

There is no clear and objective figure for the maximum closure speed ratio SR_{max}. It must be significantly smaller than 1.0, but it probably does not need to as small as 0. A speed ratio of 1.0 implies that the cavity closure line is moving with the blade; the cavity is growing nor shrinking.

When the first step of the criterion is not fulfilled, we move on to step two. The second step requires that the angle between a line tangent to the cavity closure line at a particular radius and a radial line from the center of the propeller shaft to the closure line at that radius is sufficiently large:

$$\alpha_{r,t} > \alpha_{min} \tag{2}$$

The definition of $\alpha_{r,t}$ is also shown in Figure 1. Again, there is no sound base for α_{min}. It must be significantly larger than 0°.

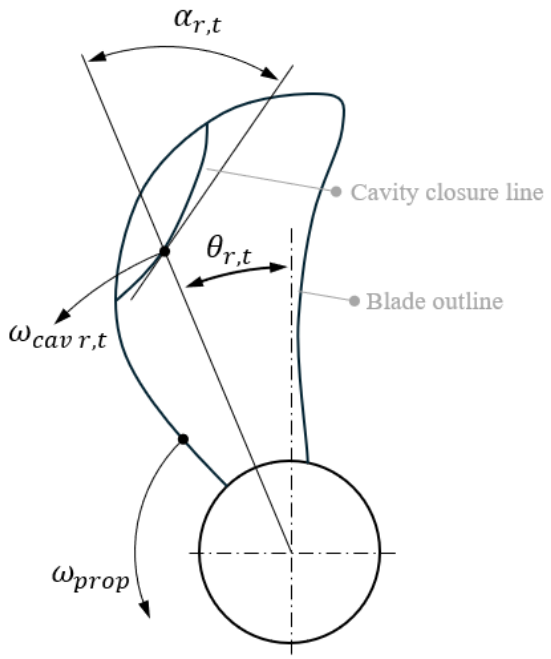


Figure 1: Definition of cavity closure line speed and angle.

Next to these two steps, there are bounds for where the criterion is applied. It is not applied above a certain radius close to the tip (we usually use 0.95R). This is because the PROCAL cavity predictions are not accurate in the very tip region because of the absence of a cavitating tip/leading edge vortex. Furthermore, it is not applied to very small cavities (chord-wise cavity length < 1% of the chord) and also not to super cavities (cavities that extend beyond the blade trailing edge).

Now the ideas that are underlying to this criterion are explained. Sheet cavitation can be erosive when the sheet sheds cavitation clouds. When these clouds collapse in a sufficiently violent manner on the same location of the propeller blade, this will lead to erosion.

The shedding of clouds is related to the occurrence of a re-entrant jet under the cavity sheet (de Lange & de Bruin, 1997), (Callenaere et al., 2001). Figure 2 shows a number of snapshots of the cyclic shedding process of a 2-dimensional cavity on a foil. On the top row we see a growing sheet cavity. The cavity closure point is moving with the flow. The cavity reaches its maximum extent on the top right-hand sketch of Figure 2. This results in a high (stagnation) pressure at the closure point, which invokes the occurrence of a re-entrant jet; a thin layer of liquid that shoots in up-steam direction between the foil surface and the vapor bubble. This is shown on the second row of Figure 2. At some point the re-entrant jet will impinge on the outer cavity surface. A cloud cavity is shed and advected by the flow. The remaining sheet cavity at the leading edge starts to grow again and the cyclic process repeats itself. This cyclic shedding process of a 2D cavity has been observed by Van Rijsbergen et al. (2012).

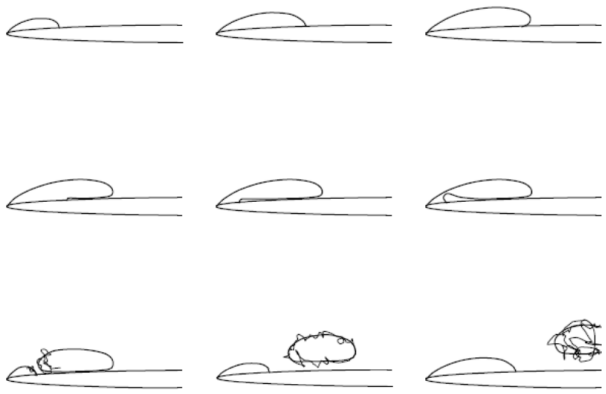


Figure 2: Cyclic shedding of a 2-dimensional cavity due to re-entrant jet impingement.

When the first step of the criterion (Equation 1) is fulfilled, this implies that the cavity is growing. The closure point is moving with the flow, there is no high pressure downstream of the cavity, and no re-entrant jet will form. Therefore, the cavity will not shed any clouds, and the cavity will be not erosive during this stage.

The cavities on the suction side of a propeller are generally not 2-dimensional. In case of a 3-dimensional cavity, the direction of the re-entrant jet is very different. It appears that the direction is more or less a reflection of the flow on the outer cavity surface in the cavity closure line (Schöön, 2000). Figure 3 shows how this would look like for the well behaving sheet cavity that was described above. The cavity closure angle $\alpha_{r,t}$ is sufficiently large. Therefore, the re-entrant jet is directed outwards, and in that case it is often called a side-entrant jet. At the tip, the jet finds an exit behind the cavitating leading edge / tip vortex. It does not impinge on the outer cavity surface, and therefore the cavity does not shed any clouds and is not erosive.

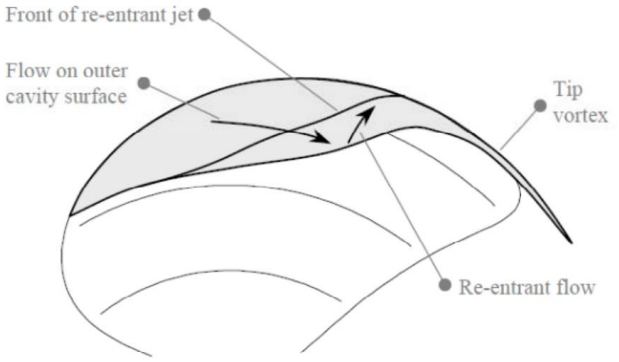


Figure 3: The direction of the re-entrant jet in case of a 3-dimensional cavity.

When $\alpha_{r,t}$ is small, the cavity will behave as a 2-dimensional cavity (at least locally). Then, it will shed clouds when it is not growing sufficiently fast. When the cavity closure angle is negative, the side-entrant jet will be directed inwards. At the hub of the blade there is no vortex that stabilizes the cavity, so cloud shedding is likely to occur.

Figure 4 shows a model-scale illustration of these phenomena. It shows the S-propeller from the thesis of Prof. Kuiper (1981) that is tested in open water in a cavitation tunnel. Due to the absence of a wake field the cavity is more or less stationary. (Variations of the cavity are only caused by variations in hydrostatic pressure.) Therefore, the first step of the criterion is not fulfilled ($SR \approx 1$). At radii smaller than 0.7R, the cavity closure angle is sufficiently large. The cavity does not shed any clouds, and the front of the re-entrant jet is clearly visible. At radii larger than 0.7R the closure angle is close to 0° or even smaller. Here the cavity sheds clouds that are potentially erosive.

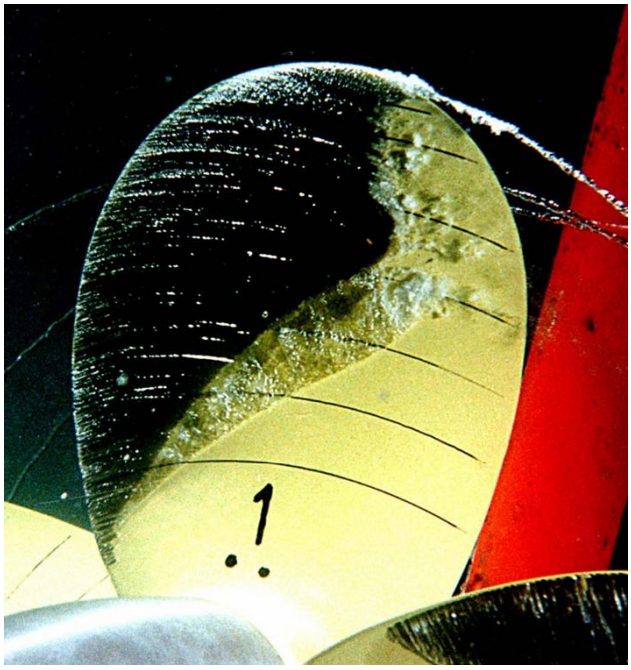


Figure 4: Cavitation on the S-propeller (Kuiper, 1981)

It also can be that the closure angle is positive at lower radii and negative at higher radii. In that case, the side-entrant jets from lower and higher radii will converge, which also results in shedding of very complex cloud structures. This behavior was observed in detail by Foeth (2008) on a twisted foil.

When the leading edge of a propeller blade rotates into the wake of the ship, the cavity often starts as an isolated cavity (i.e. a cavity that does not extend towards the tip of the blade) around 0.7R radius. Then the angle of the cavity closure line will be small or negative at the maximum radius end. Therefore, just applying the second step of the criterion is not sufficient. During this phase, the cavity is rapidly growing, and therefore it will not shed any clouds.

2.2 Pressure Side Cavitation

It is worth mentioning that the analysis function for the suction side criterion also implements a criterion for pressure side sheet cavitation. This criterion was previously presented by Moulijn et al. (2006). It is not the main topic of this paper, but the criterion is briefly described.

Pressure side cavitation was traditionally always considered erosive, and therefore it was usually avoided. However, full scale observations (Ligtelijn et al., 2004) showed that a significant amount of pressure side cavitation was present on the propellers of large container vessels, while this did not lead to erosion. Discussions in the EU project EROCAV, with important input from Prof. Göran Bark (Bark et al., 2004) led to new understanding of when pressure side cavitation is erosive or not.

Pressure side cavitation usually behaves quite different from sheet cavitation on the suction side. It does not occur when the blade rotates through the wake peak of the ship, but rather for the upwards rotating blade when the axial inflow velocity is high and the tangential inflow velocity is in the same direction as the propeller rotation. Furthermore, pressure side cavitation mainly occurs at inner radii. It usually does not extend towards the tip. Therefore, it generally does not meet the previously described criteria for suction side cavitation.

As mentioned before, sheet cavitation can be erosive when the sheet sheds cavitation clouds. When these clouds collapse in a sufficiently violent manner on the same location of the propeller blade, this will lead to erosion. However, when the sheet cavity is sufficiently two-dimensional, i.e. when the span-wise cavity extent is much larger than the chord-wise cavity extent, the cavity will be shedding clouds randomly along its span. Therefore, the implosions of these clouds will be very scattered, the collapse energy is not focusing on one location. When the cavity is also shedding naturally, which means that the collapse of the cavity (clouds) is not accelerated by a sudden load increase due to the wake field, the implosions of the scattered clouds are not very violent.

These considerations lead to two requirements that both must be met:

- The aspect ratio of the cavity, which is the span-wise cavity extent divided by the chord-wise cavity extent, must be sufficiently high.
- The cavity time ratio, which is the time from the maximum chord-wise cavity extent until cavity desinence divided by the natural shedding period of the cavity, must be sufficiently high. The shedding period is estimated using a Strouhal number based on the incoming flow velocity and the chord-wise cavity length.

More details about the pressure side cavitation criterion can be found in Moulijn et al. (2006). When this criterion is used, it provides additional design freedom over a no-pressure side cavitation constraint.

3 IMPLEMENTATION

The criteria are implemented in MARIN's MATLAB based propeller design and optimization framework PropArt (Huisman & Foeth, 2017). It uses the cavitation predictions of the Boundary Element Method (BEM) PROCAL (Vaz & Bosschers, 2006) that is ran for many propeller geometries during the propeller optimization process. The PROCAL results contain amongst others propeller forces and moments, single blade forces and moments, wetted and cavitating pressure distributions, radial distribution of circulation. For the present criteria the radial distribution of the chord-wise cavity length on the suction and pressure sides are used. The cavity thickness, which is also predicted, is not used.

Unfortunately, PROCAL is not always as robust as one would wish. The cavity lengths sometimes show oscillations between radii and also between time steps. These can easily result in a negative result of the criterion. Therefore, the cavity results are first smoothened in radial direction and in time. A simple moving average is used that is based on the current, previous and next radii and time steps.

Next step is to check if the cavity closure line between two radii meets the bounds for the criterion:

- Small cavities (< 1% of the chord) are ignored.
- Super cavities (> 100% of the chord) are also not considered.
- At the tip ($r/R > 0.95$) the criterion is not applied
- At the root ($r/R < 0.3$) the criterion is also not applied.

The propeller geometry and the cavity lengths are used to calculate the angular position of the cavity closure line (i.e. the trailing edge of the cavity) for each radius and all angular blade steps (i.e. time steps). The speed ratio of the cavity closure line (Equation 1)) is now estimated as:

$$SR_{r,t} = \frac{(\theta_{r,t+1} + \theta_{r+1,t+1}) - (\theta_{r,t-1} + \theta_{r+1,t-1})}{4 \cdot \theta_{step}} \quad (3)$$

where $\theta_{r,t}$ is the angular position of that cavity closure line at radius r and time step t and θ_{step} is the angular step between two PROCAL time steps. The average of $\theta_{r,t}$ and $\theta_{r+1,t}$ is used as this is the speed ratio for the closure line

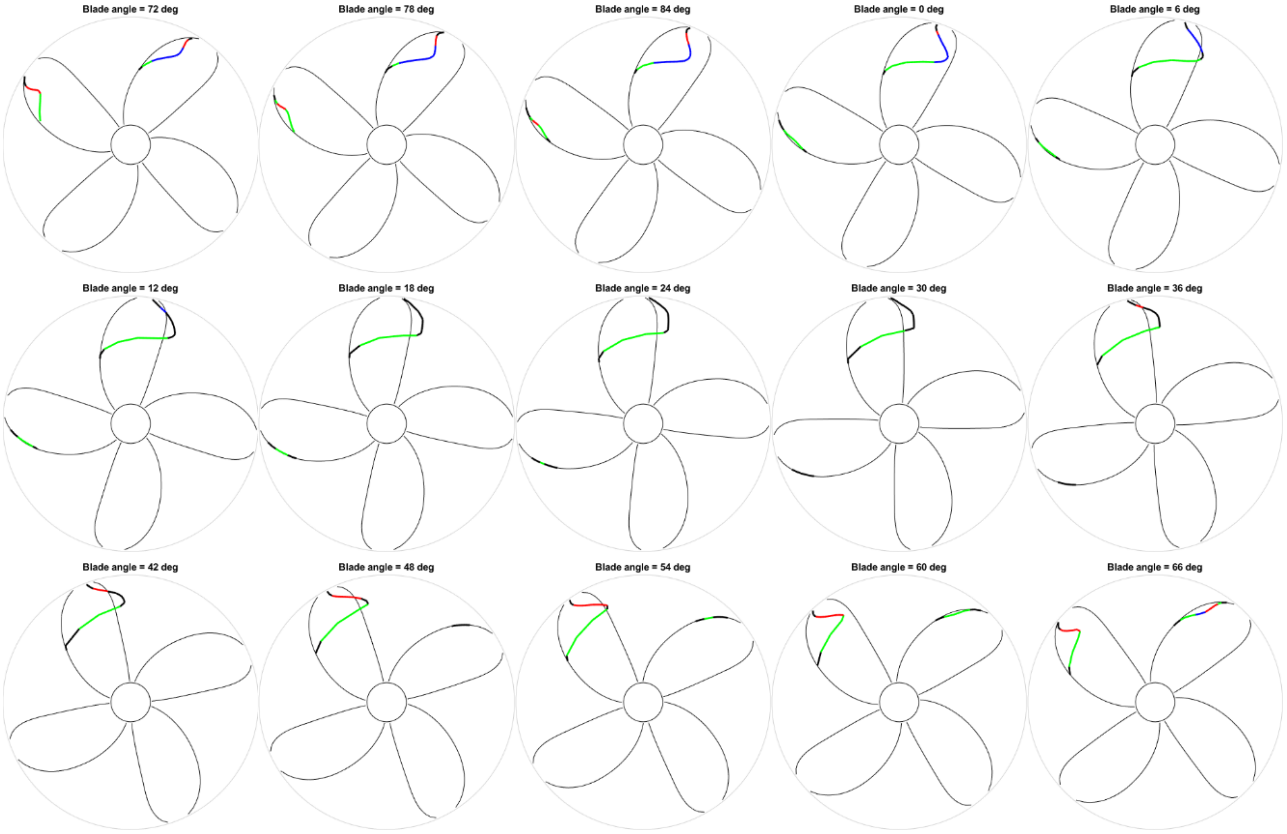


Figure 5: Cavity pattern for a propeller that has erosive cavitation

between radii r and $r+1$. The angular speed of the closure line is based on the previous and the next time step (i.e. a central difference). When this ratio is sufficiently small, the cavity is not erosive.

When the time ratio is not small, the angle between a radial line and the cavity closure line must be sufficiently large (Equation 2 and Figure 1). This closure angle is calculated as follows:

$$\alpha_{r,t} = \tan^{-1}\left(\frac{(\theta_{r,t} - \theta_{r+1,t}) \cdot (R_{r+1} + R_r)/2}{R_{r+1} - R_r}\right) \quad (4)$$

where R_r is radius r and $\alpha_{r,t}$ is the closure line angle between radii r and $r+1$ at time step t.

Sometimes, the criterion can be quite harsh, which makes it difficult to fulfill for the optimizer. When a small part of the cavity closure line only slightly exceeds the speed ratio and angle criteria this results in rejection of the design, while the risk on cavitation erosion is actually rather limited. Then it can be useful to define a cavity harm factor:

$$HF = \sum_{r,t} \left(SR_{r,t} - SR_{max}\right) \cdot \left(\alpha_{min} - \alpha_{r,t}\right) \quad (5)$$

where the summation is over all closure line elements that do not meet the criteria. This harm factor can be used as an optimization goal that must be minimized, or it can be used in a constraint that it must be less than a certain value.

4 RESULTS

Figure 5 shows an example of a cavity pattern that is considered erosive, and Figure 6 shows an example of a cavity pattern that is *not* erosive. Both figures show the outline of the blades together with the cavity closure line which is represented by the thick colored line. The meaning of the colors is as follows. A **black** line implies that the criterion is not applied as the closure line is out of bounds (e.g in case of super cavitation). A **blue** line means that speed ratio of the closure line is small. Therefore, no re-entrant jet will occur, and the cavity is not erosive. The **green** line means that the speed ratio is not small, but the angle of the cavity closure line is sufficiently large. Therefore, the re-entrant jet will be directed outwards, and the cavity is not erosive. Finally, when the closure line is plotted in **red**, the speed ratio is not small, and the angle of the closure line is such, that the re-entrant jet is expected to cause shedding of cloud cavities that can be erosive.

The shrinking sheet cavity on the downwards rotating blade in Figure 5 is considered particularly erosive. This sheet will shed clouds at the location where it has its maximum chord-wise extend, close to the point where the green line turns red. The collapse energy of these clouds will focus on the same radial location on the blade for every revolution, which will eventually result in erosion of the blade surface.

Also in the non-erosive cavity we see a cavity that has its maximum chord-wise extent in the mid-span. This occurs on the top row of Figure 6, just before the blade reaches the top position at a radius around 0.8R. In this case the cavity is not erosive because the speed ratio of the cavity closure line is small. The cavity is growing with respect to the blade. No re-entrant jet will occur, and therefore the cavity is not considered erosive.

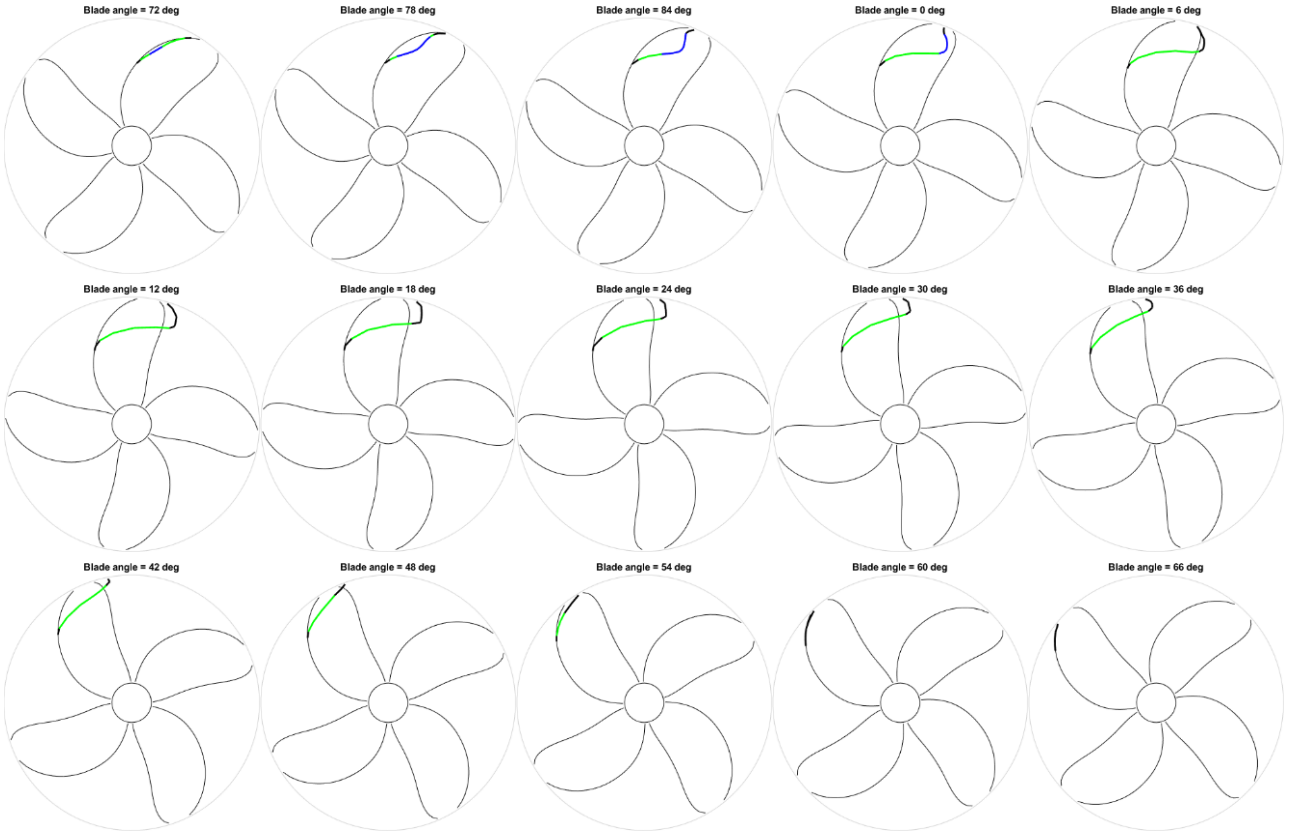


Figure 6: Cavity pattern for a propeller that has non-erosive cavitation

The method was applied to a number of propellers for which the erosiveness of the cavitation was known from full scale observations or model experiments. This did not lead to clear conclusions on whether this method can correctly distinguish between erosive or not erosive cavitation. Sometimes, the criterion is right, but other times it is not. The number of suitable and available cases was also limited.

5 APPLICATION

The method is more successful when it is applied in an automated design process. This section presents an application in a relatively simple optimization task. The optimization is done by means of MARIN's propeller design and optimization framework PropArt (Huisman & Foeth, 2017).

Table 1 presents the main design starting points for the optimization exercise, and Figure 7 shows the wake field for the propeller.

There are two goals:

1. The propeller efficiency must be maximized
2. The underwater radiated noise (URN) must be minimized

The first goal is obvious. A propeller always must have the highest possible efficiency. The second goal was selected as it drives towards propeller designs that have a strongly reduced loading at the tip, which involves a risk for erosive cavitation.

Table 1: Design starting points

Parameter	Value
Ship speed [Kn]	14
Propeller rotation rate [RPM]	102
Propeller thust [kN]	675
Number of blades	4
Propeller diameter [m]	6.0
Hub diameter [m]	1.0
Propeller shaft submersion [m]	3.6

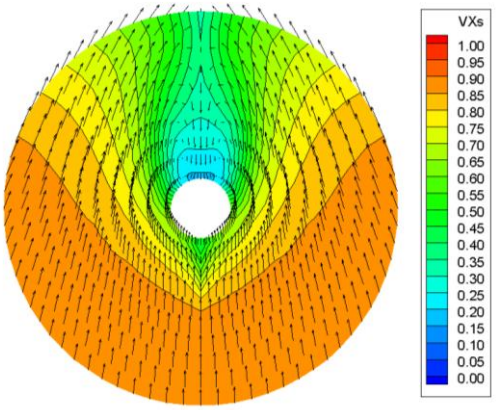


Figure 7: Wake field for design exercise

Both goals are calculated by PROCAL (MARIN's BEM code for propeller analysis). The URN is calculated by the Empirical Tip Vortex (ETV) method (Bosschers 2018) that relates the URN of the tip vortex to the propeller blade load in terms of circulation at 0.95R radius. In reality, the sheet cavitation will also contribute to the URN, but this is not considered in the present exercise.

Next to these goals, the following constraints are applied:

1. The margin against mid-chord cavitation must be higher than 10% on σ_n. This is expressed mathematically as $-C_{pn} < 0.9 \cdot \sigma_n$, where C_{pn} is the minimum non-dimensional pressure coefficient in the mid-chord area and σ_n is the cavitation number (both based on the propeller rotation rate).
2. No face cavitation. This is achieved by requiring that the pressure at the leading edge on the face of the blade is higher than the vapor pressure.
3. No erosive suction side sheet cavitation according to the cavity planform criterion.

First, an optimization is done with only constraints 1 and 2 active. Then the optimization is repeated with all constraints.

Table 2 presents the geometric parameters that are varied during the optimization. A modest amount of geometric freedom is allowed. The parameters were selected to have a simple yet relevant example. The pitch distribution is one of the most important parameters for both goals: efficiency and URN. Next to the pitch, camber has a strong influence on cavitation. The skew is important for the blade leading edge contour, which has an important influence on the shape of the cavity closure line. The chord distribution is fixed, but the chord lengths can be varied through the blade area ratio. The rake, blade thickness and blade section thickness and camber distributions were fixed.

Table 2: Geometric design freedom

Parameter	Min	Max
Expanded blade area ratio	0.4	0.6
Pitch reduction @ hub	0.0	0.5
Radius max pitch	0.5	0.8
Pitch reduction @ tip	0.0	0.7
Pitch shape factor tip	0.0	0.6
Skew extent angle	5°	25°
Skew bisector angle	-5°	10°
Camber / chord @ hub	0.0	0.1
Camber / chord @ 0.7R	0.0	0.05
Camber / chord @ tip	-0.02	0.03

For the present exercise the Competitive Multi Objective Particle Swarm Optimization (CMOPSO) algorithm by Zang et al. (2018) is used. This is the default optimizer of PropArt. The method was updated to handle constraints (Foeth & Bosschers, 2026). The population is updated by first adding the last evaluated generation and retaining the best half based on the Pareto rank (elitism). Next, each particle's input parameters are updated by adding a velocity vector comprised of three components. The first component is the difference in input parameters between the current particle and a leader particle; the competitive element is introduced by not taking a single leader particle but first taking a random pair from the ten particles with the best Pareto rank and then selecting the one closest in terms of goal values. The second component is the particle's velocity from its previous incarnation. Both these components are scaled by a uniform random number per parameter. The third component is a polynomial mutation step whereby each input parameter has a small chance to be modified, identical to the mutation phase in NSGA-II (Deb, 2002).

Figure 8 shows the optimization progression in terms of the two goals (propeller efficiency and URN source level) for the first optimization where only constraints 1 and 2 were active. Each dot represents a propeller that was evaluated, where the color indicates the generation of the propeller. Actually, these results follow from two separate optimizations. During the first 50 generations, the geometry freedom was smaller (the maximum pitch reduction @ tip was 0.5 instead of 0.7 amongst others). This appeared to be a strong limitation. Therefore the freedom was increased and the optimization was continued for 50 additional generations, starting from the results after 50 generations. The result after 50 generations was more or less located at the rather sharp line between light blue and yellow dots.

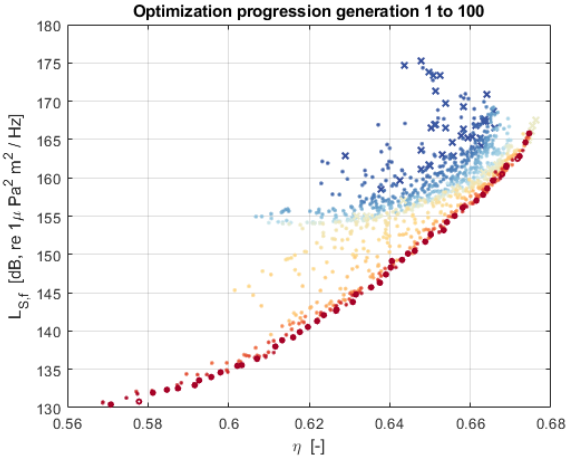


Figure 8: Optimization progression with constraints 1 and 2

Figure 8 clearly shows how the optimization converges towards a pareto front that represents the trade-off between efficiency and URN. On the top right corner we find propellers with a high efficiency and a high URN source level. On the bottom left corner we find propellers with a low URN source level and a low efficiency.

Figure 9 shows a comparison of the pareto fronts of the optimizations without and with the cavitation erosion criterion. This figure clearly shows the impact of the

erosion constraint on the pareto front. The optimizer cannot find feasible propellers (i.e. propellers that fulfil the criterion) in the lower left corner.

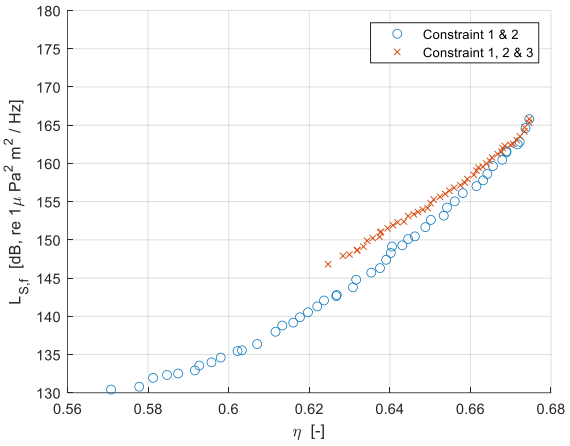


Figure 9: Comparison of pareto fronts without and with cavitation erosion criterion

Indeed all propellers on the *Constraints 1, 2 and 3* front fulfil the criterion. Figure 6 shows the cavitation pattern on one of these propellers. Figure 5 shows the cavitation pattern on one of the propellers on the *Constraints 1 and 2* front. There are a few propellers on the *Constraints 1 and 2* front that fulfil, or almost fulfil, the criterion. These propellers are located in the top right corner where the front of both optimizations coincide. However, most propellers on the *Constraints 1 and 2* front show a cavity pattern like in Figure 5.

Figure 10, Figure 11, Figure 12 and Figure 13 show a selection of the geometry parameters for the propellers on the Pareto front.

Figure 10 plots the radial location where the maximum pitch occurs as function of the first optimization goal (efficiency). For the propellers with high efficiency, the maximum pitch occurs at a high radius. In case of *Constraint 1 &2*, the radial location of maximum pitch is limited by the upper bound of this parameter (see Table 2).

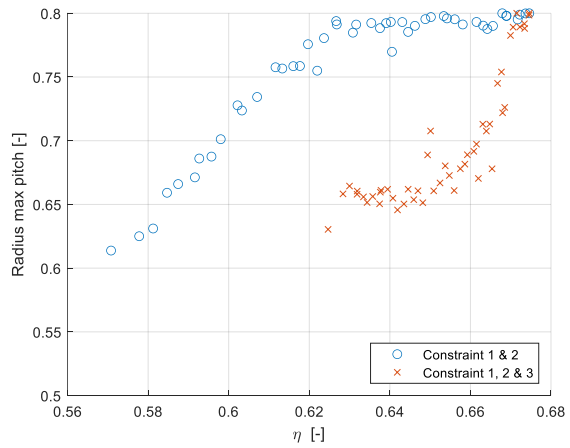


Figure 10: Radial location of the maximum pitch for the propellers on the pareto front

Figure 11 plots the reduction of the pitch at the tip as function of efficiency. Again the propellers on the *Constraint 1 &2* front hit the upper bound of the pitch reduction @ tip parameter, this time for low efficiency.

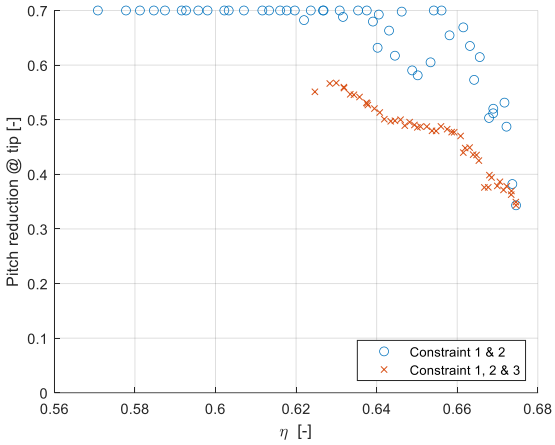


Figure 11: Pitch reduction at the tip for the propellers on the pareto front.

When the suction side sheet cavitation erosion criterion (Constraint 3) is applied, this limits the unloading of the tip. For too strong pitch reduction (< 0.55) no feasible propellers that fulfil the criterion are found. Furthermore, the radial location of maximum pitch is moved to lower radii in order to avoid isolated cavities around 0.8R like in Figure 5.

Figure 12 and Figure 13 plot the camber at 0.7R and at the tip, again as function of the efficiency. When constraint 3 is applied, the camber at 0.7R is slightly higher. This is probably to control (avoid) cavitation at lower radii, but the camber is limited by either the margin against mid-chord cavitation or the no pressure side cavitation constraint.

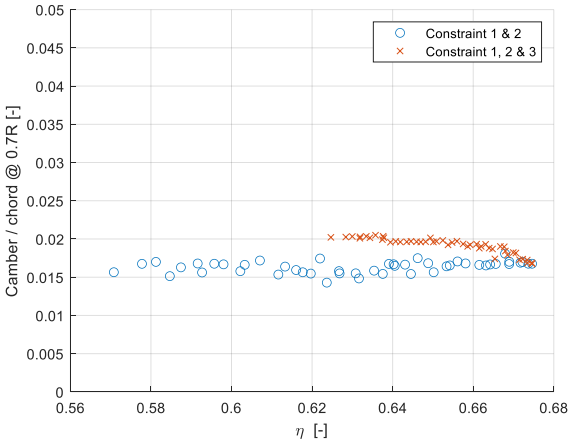


Figure 12: Camber at 0.7R radius for the propellers on the pareto front

It is remarkable that negative camber ratios at the tip are found to be optimal for many propellers (see Figure 13). Only the propellers at the high efficiency end have positive camber at the tip. A negative camber reduces the circulation at the tip and therewith the strength of the tip vortex. Therefore, this is beneficial for the URN source

level of the tip vortex. Furthermore, it also may help to increase the angle of closure line in the tip region by stabilizing the cavitation.

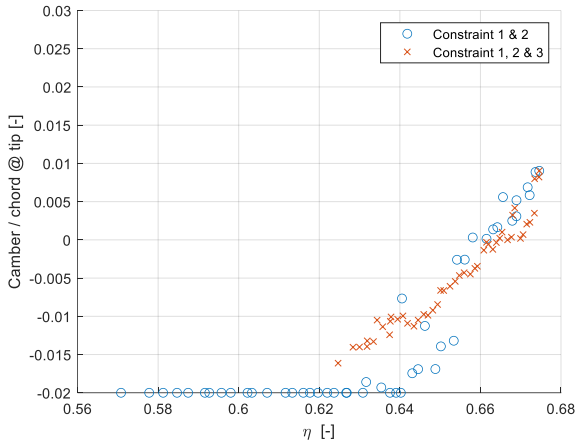


Figure 13: Camber at the tip for the propeller on the pareto front

There is much to be said against this simple application exercise. There are no constraints that limit the amount of cavitation or optimization goals that strive to reduce the amount of cavitation or hull pressure fluctuations. This explains the rather large cavities in Figure 5 and Figure 6. The URN source level is based on the ETV model (Bosschers, 2018) for tip vortex cavitation. Other cavitation forms, like sheet cavitation, will also generate noise, although the tip vortex is often the dominating noise source. Furthermore, only positive circulation at the tip is considered. This explains why the optimization finds rather extreme pitch reductions at the tip. This may results in negative circulation at the tip, leading to a pressure side tip-vortex.

The purpose of this application example is, however, is to give a clear and easy to understand example of why a cavitation erosion criterion is needed, and how it influences the optimization results. Foeth & Bosschers (2026) present an example of a more complete propeller design optimization that also includes the present erosion criterion. At MARIN, the criterion has been applied successfully in many propeller design projects.

6 CONCLUSION

This paper presented a practical method to assess the risk on cavitation erosion during an automated propeller design process. The underlying ideas were discussed and the details of the implementation were presented. The method is too simple to accurately distinguish between erosive and non-erosive cavitation for existing cases. However, when it is applied in a propeller design optimization, it can effectively prevent the optimization process from converging towards propeller designs with obviously erosive cavitation at very limited computational cost.

ACKNOWLEDGEMENT

The Cooperative Research Ships (CRS), and in particular the CRS EROSION, PROPAGATE and PROPAGATE II working groups, are acknowledged for their support in this research.

REFERENCES

Bark, G., Berchiche, N. & Grekula, M. (2004), Application of principles for observation and analysis of eroding cavitation - The EROCAV observation handbook, Department of Naval Architecture and Ocean Engineering, CHALMERS UNIVERSITY OF TECHNOLOGY, SE- 412 96 Göteborg, Sweden.

Bosschers, J. (2018), Propeller Tip-Vortex Cavitation and its Broadband Noise, PhD thesis, University of Twente, ISBN: 978-94-92679-52-9

Callenaere, M, Franc, J.P., Michel, J.M. & Riondet, M. (2001), 'The cavitation instability induced by the development of a re-entrant jet', Journal of Fluid Mechanics, 444: 223-256. 10.1017/ S0022112001005420. hal-00212301

Dep, K. (2002), 'A Fast and Elitist Multi-objective Genetic Algorithm: NSGA-II', IEEE Transactions on evolutionary computation, vol. 6(2)

Foeth, E.J. (2008), The structure of Three-Dimensional Sheet Cavitation, PhD thesis, Delft University of Technology, ISBN: 978-90-6464-236-4

Foeth, E.J. & Bosschers, J. (2026). 'Design optimization study for a low-noise propeller for a container ship', Proceedings of the 9th International Symposium on Marine Propulsors, smp'26, St. Johns, Canada.

Gypa, I., Jansson, M., Wolf, K. & Bensow, R. (2023), 'Propeller Optimization by Interactive Genetic Algorithms and Machine Learning', Ship Technology Research, 70(1): 56–71, https://doi.org/10.1080/09377255.2021.1973264.

Huisman, J. & Foeth, E-J. (2017). 'Automated multi-objective optimization of ship propellers', Ninth International Symposium on Marine Propulsors smp'29, St. John's, NL, Canada

Huisman, J., Looijenga, J., & Leslie-Miller, M. (2024). ' Propeller design for propulsion and regeneration', 28th International HISWA Symposium, Amsterdam, The Netherlands.

Kuiper, G. (1981), Cavitation Inception on Ship Propeller Models, PhD thesis, Delft University of Technology.

Lange, D.F. de and Bruin, G.J. de (1997). 'Sheet cavitation and cloud cavitation, re-etrant jet and three-dimensionality', Applied Scientific Research, 58: 91-114.

Ligtelijn, J.T., Wijngaarden, H.C.F. van, Moulijn, J.C. & Verkuyl, J.B. (2004), 'Correlation of Cavitation: Comparison of Full-Scale Data with Results of Model Tests and Computations', SNAME Annual Meeting, Washington DC, USA.

Melissaris, T., Bulten, N. & Oprea, I (2019), 'The necessity of accurate prediction of cavitation behaviour for fuel efficient propellers', Sixth International Symposium on Marine Propulsors smp'19, Rome, Italy.

Moulijn, J.C., Friesch, J., Genderen, M. van, Junglewitz, A & Kuiper, G. (2006), 'A Criterion for the Erosiveness of Face Cavitation', Sixth International Symposium on Cavitation CAV2006, Wageningen, The Netherlands.

Rijsbergen, M. van, Foeth, E.J., Fitzsimmons, P. & Boorsma A. (2012), 'High-Speed Video Observations and Acoustic-Impact Measurements on a NACA 0015 foil', Proceedings of the Eighth International Symposium on Cavitation (CAV 2012), Singapore.

Schenke, S., Melissaris, T. & Terwisga, T.J.C. van (2019), 'On the Relation between the Potential Cavity Energy and the Acoustic Power Signature caused by Periodic Vapor Cavity Collapses', Sixth International Symposium on Marine Propulsors smp'19, Rome, Italy.

Schöön, Johannes (2000), A Method for the Study of Unsteady Cavitation: Observations on Collapsing Sheet Cavities, Doktorsavhandlingar Vid Chalmers Tekniska Högskola, N.S., 1587 (Göteborg).

Vaz, G. & Bosschers, J. (2006). 'Modeling Three-Dimensional Sheet Cavitation on Marine Propellers using a Boundary Element Method'. Sixth International Symposium on Cavitation CAV2006, Wageningen, The Netherlands.

Vesting, F. (2015), Marine Propeller Optimisation: Strategy and Algorithm Development, Doktorsavhandlingar Vid Chalmers Tekniska Högskola, N.S., 3944 (Göteborg).

Zhang, X, Zheng, X., Cheng, R., Qiu, J. & Jin, Y. (2018), 'A Competitive Mechanism Based Multi-Objective Particle Swarm Optimizer with Fast Convergence', Information Sciences, 427: 63–76, https://doi.org/10.1016/j.ins.2017.10.037.